SLO2.1/NALCN Functional Complex Activity in Mouse Myometrial Smooth Muscle Cells During Pregnancy.

Running tittle: Role of SLO2.1/NALCN During Pregnancy.

Authors:
Juan J. Ferreira* and Lindsey N. Kent*, Ronald McCarthy, Alice Butler, Xiaofeng Ma, Nikita Peramsetty, Chinwendu Amazu, Alexander Zhang, Grace C. Whitter, Sarah K. England** and Celia M. Santi**
Department of Obstetrics and Gynecology, Center for Reproductive Health Sciences, Washington University in St. Louis, School of Medicine, 425 S. Euclid Avenue, CB 8064, St. Louis, MO 63110, USA

*These authors contributed equally
**Correspondence: englands@wustl.edu (S.K.E.), and santic@wustl.edu (C.M.S.)

Acknowledgments.
We thank Dr. Deborah Frank for critical review of the manuscript. This work was supported by National Institutes of Health grant R01HD088097 (to C.M.S. and S.K.E.), and the Department of Obstetrics and Gynecology at Washington University in St. Louis.

Author contributions.
J.J.F., L.N.K., R.M, A.B, X.M., N.P, C.A., A.Z, G.W, S.K.E., and C.M.S. designed, performed, and analyzed the experiments. J.J.F. and L.N.K. prepared figures. J.J.F., L.N.K., S.K.E., and C.M.S. drafted the manuscript. J.J.F., L.N.K., R.M, A.B, X.M., N.P, C.A., A.Z, G.W, S.K.E., and C.M.S, edited, revised, and approved the final version of the manuscript.

Conflict of Interests: Authors declare no conflict of interests.

Keywords: SLO2.1 Channels, NALCN Channels, Myometrium, Pregnancy, Uterine Contractions

Data Availability Statement: The data generated and analyzed during the current study are available from the corresponding author upon reasonable request.

Joint first and senior authorship: Juan Ferreira and Lyndsey Kent should be considered joint first author and Sarah K. England and Celia M. Santi should be considered joint senior author.

Abstract.
At the end of pregnancy, the uterus transitions from a quiescent to a highly contractile state. This is partly due to depolarization of the resting membrane potential in uterine (myometrial) smooth muscle cells (MSMCs). Experiments with human MSMCs showed that the membrane potential is regulated by a functional complex between the sodium (Na^+)-activated potassium (K^+) channel SLO2.1 and the Na^+ Leak Channel Non-Selective (NALCN). In human MSMCs, Na^+ entering through NALCN activates SLO2.1, leading to K^+ efflux, membrane hyperpolarization (cells become more negative inside), and reduced contractility. Decreased SLO2.1/NALCN activity results in reduced K^+ efflux, leading to membrane depolarization, Ca^{2+} influx via voltage-dependent calcium channels, and increased MSMC contractility. However, all of these experiments were performed with MSMCs isolated from women at term, so the role of the SLO2.1/NALCN complex early in pregnancy was speculative. To address this question here, we examined the role of the SLO2.1/NALCN complex in regulating mouse MSMC membrane potential across pregnancy. We report that *Slo2.1* and *Nalcn* expression change along pregnancy, being more highly expressed in MSMCs from non-pregnant and early pregnant mice than in those from late-pregnant mice.
Functional studies revealed that SLO2.1 channels mediate a significant portion of the K^+ current in mouse MSMCs, particularly in cells from non-pregnant and early pregnant mice. Activation of SLO2.1 by Na^+ influx through NALCN led to membrane hyperpolarization in MSMCs from early pregnancy but not in MSMCs from later pregnancy. Moreover, we found that the NALCN/SLO2.1 complex regulates intracellular Ca^{2+} responses more in MSMCs from non-pregnant and early pregnancy mice than in MSMCs from late pregnancy. Together, these findings reveal that the SLO2.1/NALCN functional complex is conserved between mouse and humans and functions throughout pregnancy. This work could open avenues for targeted pharmacological interventions in pregnancy-related complications.

1. Introduction

During much of pregnancy, the uterus is in a quiescent phase. At term, the uterus becomes highly contractile to expel the fetus (Casteels & Kuriyama, 1965; Parkington et al., 1999). Uterine contractility is partially controlled by myometrial smooth muscle cell (MSMC) excitability, which is regulated by the MSMC resting membrane potential (Vm) (Ferreira et al., 2019, 2021; Parkington et al., 1999; Reinl et al., 2015a, 2018). The Vm is maintained through a balance between hyperpolarizing forces, primarily driven by outward potassium (K^+) currents (Anwer et al., 1993; Knock et al., 1999), and depolarizing forces, largely mediated by inward sodium (Na^+) leak currents. Changes in these ion fluxes modify the Vm and modulate calcium (Ca^{2+}) influx through voltage-dependent Ca^{2+} channels (VDCCs) and other Ca^{2+} channels such as TRP C1, 3, and 6 (Babich et al., 2004; Dalrymple, 2002; Dalrymple et al., 2007; Ku et al., 2006; Lacampagne et al., 1994; Wang et al., 2020; Yang & Sachs, 1989).

Human MSMCs isolated from non-laboring women at term exhibit an Na^+-regulated K^+ current (K_{Na}) that is lost when the K^+ channel SLO2.1 is knocked down. The current through SLO2.1 hyperpolarizes the MSMC Vm and dampens excitability (Ferreira et al., 2019). SLO2.1 is activated by Na^+ influx through sodium leak channel nonselective (NALCN). This was demonstrated by showing that inhibition of NALCN with gadolinium

(Gd^{2+}) or replacing Na^+ with Lithium (Li^+), which can pass through NALCN but not activate SLO2.1, prevented Na^+-activated K^+ influx. Furthermore, NALCN and SLO2.1 are in proximity to one another in human MSMCs, and functional coupling of NALCN and SLO2.1 regulates contractility (Ferreira et al., 2021). These data support a model that, during pregnancy, Na^+ influx through NALCN activates SLO2.1, leading to K^+ influx, Vm hyperpolarization, and MSMC quiescence. However, all these experiments were done with MSMCs from women at term, so the functional interactions between SLO2.1 and NALCN earlier in pregnancy are unknown.

In this study, we investigated the SLO2.1/NALCN complex dynamics in a mouse model that allows for the dissection of the complex's function at various stages of pregnancy. We present evidence suggesting that the regulation of uterine excitability through the SLO2.1/NALCN functional complex is conserved across species, underscoring its evolutionary significance. Moreover, we demonstrate the relevance of this mechanism throughout different stages of pregnancy. Our findings reveal differential expression of both SLO2.1 and NALCN channels in mouse MSMCs at various pregnancy stages, with a notable decrease in mRNA expression towards late pregnancy, corresponding to the heightened MSMC excitability observed during this period. Furthermore, our data indicate a reduction in the functional expression of SLO2.1 currents and SLO2.1/NALCN complex activity in mouse MSMCs towards late pregnancy, further supporting our observations.

Methods

2.1. Animals and tissue collection. Animal procedures followed NIH guidelines and were approved by the Animal Studies Committee at Washington University. C57BL/6 mice (Jackson Laboratories) were housed in 12-hour light/dark cycle with ad libitum food and water. Each female mouse aged 8-22 weeks was housed with a male aged 8-22 weeks and checked every morning. The day on which a copulatory plug was detected was recorded as pregnancy day 0.5. Uteri were collected from non-pregnant mice at different stages of estrus and from pregnant mice at gestational days 7.5, 10.5, 14.5, and 18.5.

2.2. RNA isolation, reverse transcription, and real time PCR. To isolate total RNA from primary mouse MSMCs and hTERT-HM cells, the Qiagen RNeasy Kit (catalogue no. 74124; Qiagen, Valencia, CA) was used. Superscript III Reverse Transcriptase (catalogue no. 18080-044; Invitrogen, Carlsbad, CA) and random hexa-nucleotide primers (catalogue no. H0268-1UN; Sigma-Aldrich, St Louis, MO) were used to synthesize cDNA. PCR primers (Integrated DNA Technologies, Coralville, IA) were designed with Oligo 7 software (Molecular Biology Insights, Colorado Springs, CO). RNA was extracted from uterine tissue with Trizol and the aurum total RNA fatty and Bio-rads fibrous tissue module. iScript reverse transcription supermix was used to synthesize cDNA. Real-time PCR was performed with iQ-SYBR Green Supermix on a CFX96 Real-time System in the following conditions: 95°C for 5 minutes, then 50 cycles of 95°C for 10 seconds and 60°C for 30 seconds. Reactions were performed in duplicate, and data were normalized to Top1 and Sdha using the delta-delta CT method. Primer sequences: *Nalcn*, 5'TTTCCCCGCTGGCGCTCCTA3' and 5'ACCAGCTGCCAACCACCAGC3'; *Top1*, 5'AAGATCGAGAACACCGGCATA3' and 5' CTTTTCCTCCTTTCGTCTTTCC3'; *Sdha*, 5'GGAACACTCCAAAAACAGACCT3' and 5'CCACCACTGGGTATTGAGTAGAA3'

(Reinl et al., 2018); *Slo2.1*, 5'TCTTGAGAGCATGGGCTGTG3' and 5'GGTGACTGCTGCCCTTCTTG3'.

2.3. Immunohistochemistry. Uteri were fixed in 10% buffered formalin, processed, and sectioned (4 µm). Slides were incubated in citric acid-based solution at ~95°C for 30 min, blocked with Avidin/Biotin kit and 10% normal goat serum (GS) for 30 min, and incubated overnight at 4°C in primary antibodies (1:500 anti-NALCN, Alomone labs; 1:4000 anti-SLO2.1, Absolute Antibody; 1:50 alpha-Smooth muscle actin, Invitrogen). Slides were incubated in biotinylated secondary antibodies in 10% GS for 30 min at room temperature. Slides were washed three times with PBS between each step except for after the block. Signal was detected with Vectastain Elite ABC and DAB substrate kits. Nuclei were counterstained with Gills Hematoxylin. Images were captured on a Leica TCS SPE microscope.

2.4. Electrophysiology. Cells were serum starved in DMEM for at least 2 hours before patch clamp experiments. Borosilicate glass pipettes (Warner Instruments, Hamden, CT) with 1.0–1.8 megaohm resistance were used for whole-cell recordings, and pipettes with 4–6 megaohm resistance were used for single-channel recordings. Whole-cell recordings of mouse MSMCs were performed in asymmetrical K^+ solutions (unless specified in the figures) as follows (in mM): External solution 135 NaCl (replaced by 135 LiCl, in the Na-free or 0 mM Na^+ solution), 5 KCl, 5 Hepes, 2 $MgCl_2$; Internal solution, 140 KCl, 5 Hepes, 0.5 $MgCl_2$, 5 ATPMg (0.6 mM free Mg^{2+}) and 10 EGTA (0 Ca^{2+} solution), or 1 EGTA and 100 nM Ca^{2+} free (Ca^{2+}-containing solution). The pH of all solutions was adjusted to 7.3-7.4. During experiments, cells were continuously perfused. Traces were acquired with Axopatch 200B (Molecular Devices, Sunnyvale, CA), digitized at 10 kHz for whole-cell recordings. Records were filtered at 2 kHz for macro whole-cell currents. Data were analyzed with pClamp, version 10.6 (Molecular Devices) and SigmaPlot, version 15 (Systat Software Inc., Chicago, IL).

2.5. *In situ* proximity ligation assay. Mouse MSMCs were cultured in 8-well chambered slides and serum-deprived in 0.5% FBS for 24 hours. Cells were then washed in ice-cold 1X PBS, fixed with 4% paraformaldehyde in PBS for 20 minutes at room temperature, washed 4 x 5-minutes in 1X PBS, permeabilized with 0.1% NP-40 for 5 minutes at room temperature, washed twice with PBS and once with 100 mM Glycine in PBS, and rinsed in milliQ water. Duolink i*n situ* proximity ligation assay (PLA) labeling was performed with NALCN (mouse monoclonal, 1:100, StressMarq) and SLO2.1 (rabbit polyclonal, 1:200, Alomone) antibodies. The manufacturer's protocol was followed except that cells were stained with NucBlue Fixed Cell Stain Ready Probes (Invitrogen) for 5 minutes at room temperature before the final wash in wash buffer B. Slides were dried at room temperature in the dark, mounted in Vectashield, and stored at -20°C until analysis. Images were captured with a Leica AF 6000LX system with a Leica DMi8000 inverted microscope, a 63X objective (HC PL FluoTar L 63X/0.70 Dry), and an Andor-Zyla-VCS04494 camera at room temperature. Excitation wavelengths were 488 nm for PLA signals and 340 nm for NucBlue. Leica LasX software controlled the system and collected data. Acquisition parameters were: 2- and 1.5-seconds exposure time for 488 nm and 340 nm, respectively, no binning, 2048 x 2048 pixels resolution, and a voxel size of 0.103 mm. Image analysis was performed with LAS X and ImageJ software, as well as SigmaPlot 15. Data are reported as the number of punctae per cell after background subtraction.

2.6. Determination of Vm by flow cytometry. Mouse MSMCs were centrifuged at 325 RCF for 5 min and resuspended in modified Ringer's solution (80 mM Choline Cl, 10 mM HEPES, 5 mM Glucose, 5 mM KCl, 2 mM $CaCl_2$, pH 7.4). Before recording, 0.02 mg/ml Hoechst and 150-500 nM DiSC3(5) were added to 500 µl of cell suspension. Data were recorded as individual cellular events based on Side Scatter Area (SSC-A) and Forward Scatter Area (FSC-A), with fluorescence collected from 10,000-25,000 events per condition. Thresholds for FSC-A and SSC-A were set to exclude signals from cellular debris. Living cells were selected with the Pacific Blue filter (450nm), and DiSC3(5)-positive cells were detected with the Allophycocyanine APC filter (670 nm).

To measure the effect of Na^+ on Vm, 80 mM NaCl or Lithium (Li^+) was added to the 500 µl suspensions. At the end of each experiment, 1 µM Valinomycin was added to establish a reference point for cross-experiment comparisons. Normalization was calculated as $((F_{Valino} - F_{Ref})/(F_{Valino} - F_{Cation}))*100$, where F_{Ref} is the median fluorescence of the population in the basal condition, F_{Cation} is after addition of the cation, and F_{Valino} is after addition of Valinomycin. Data were analyzed with FlowJo 10.6.1 software and reported as median values.

2.7. Lentivirus production and injection. *Scrambled*, *Slo2.1,* and *Nalcn* shRNAs were cloned into the pGFP-C-shLenti vector (OriGene) and co-transfected with pMD2.G and psPAX2 (Addgene, plasmid # 12259 and 12260) into HEK293T cells to produce virus. Media from transfected HEK293T cells was collected and concentrated with Lenti-X concentrator. Lentiviruses were injected into multiple sites along the uterine horn in non-pregnant mice, and MSMCs were isolated 7-10 days later. EGFP positivity was used to identify MSMCs expressing the shRNAs. The following shRNA sequences were used: *Slo2.1,* TCTAACTTGGCCTTTATGTTTCGACTGCC and AGAGCCATTCAGCGTACACAGTCTGCAAT; *Nalcn,* TGGTGACTGTGGATGTAATAGTTGCTGCC and AACAGGACACCTGCTGTCTCTTCAGAATC.

2.8. Calcium imaging. Cells were cultured on glass coverslips for 16-24 hours at 37 °C, incubated in 2 µM Fluo-4 AM and 0.05-0.1% Pluronic Acid F-127 in Opti-Mem for 60-90 min, then incubated in Ringer's solution for 10 to 20 minutes. Solutions were applied with a perfusion system with an exchange time of approximately 1.5 seconds. Recordings began 2-5 minutes before addition of test solutions. Ionomycin (2-5 µM) was added at the end of recordings as a reference point for comparison across experiments. Calcium (Ca^{2+}) signals were recorded using a Leica AF 6000LX system with a Leica DMi8000 inverted microscope, a 40X (HC PL FluoTar L 40X/0.70 Dry) or a 20X (N-Plan L 20X/0.35 Dry) air objective, and an Andor-Zyla-VCS04494 camera. Excitation and emission filters were 488/20 nm and 530/20 nm, respectively. Leica LasX2.0.014332 software-controlled image collection. Acquisition parameters: 120 ms exposure time, 2x2 binning, 512 x 512 pixels resolution, with a voxel size of 1.3 mm for the 20X objective. Images were captured every 10 seconds. Data were analyzed with LAS X, ImageJ, Clampfit 10 (Molecular Devices), and SigmaPlot 15 software. Changes in intracellular Ca^{2+} concentration are presented as (F/F_{Iono}) after background subtraction. All imaging experiments were conducted at room temperature. Cells were considered responsive if they exhibited fluorescence changes of at least 5-10% of ionomycin responses after normalization.

2.9. Statistical analysis. Statistical analyses were performed in SigmaPlot, version 15.0. For independent samples, an unpaired Student's t-test was used. In experiments with case-control designs involving the same individuals, a paired t-test was used. A one-way ANOVA or multiple comparison tests were used for comparisons between multiple populations. Results are expressed as mean ± standard deviation (SD), with $P < 0.05$ considered statistically significant.

2. Results

3.1. SLO2.1 and NALCN are expressed in mouse myometrial smooth muscle cells. To determine whether SLO2.1 and NALCN are expressed in mouse MSMCs as they are in human MSMCs, we first performed qRT-PCR to examine expression of the related channels *Slo2.1* and *Slo2.2*. We could only detect *Slo2.1* mRNA in MSMCs isolated from non-pregnant mice and mice at different stages of pregnancy (Figure 1a, b). We also found that *Slo2.1* and *Nalcn* expression was significantly higher in uteri of non-pregnant mice and uteri from day post-copulation 7.5 (d7.5) mice than in uteri from mice at term (d18.5) (Figure 1c, d). Immunohistochemistry showed that, in non-pregnant mice, SLO2.1 and NALCN proteins were expressed in the longitudinal and circular smooth muscle layers (Figure 1e). On d7.5, SLO2.1 and NALCN were evident in both mesometrial and antimesometrial myometrial smooth muscle at both implantation and inter-implantation sites. However, NALCN was more abundant in the antimesometrial myometrium than in the mesometrial myometrium. At d14.5 and d18.5, SLO2.1 and NALCN expression in smooth muscle appeared lower than at d7.5. Staining for smooth muscle actin confirmed that SLO2.1 and NALCN were predominantly expressed in smooth muscle. Staining in the decidua was largely non-specific background (Supplementary Figure 1). These findings indicate that SLO2.1 and NALCN are expressed in mouse MSMCs, and that expression decreases late in pregnancy.

3.2. Mouse myometrial smooth muscle cells conduct a Na^+-activated K^+ current (K_{Na}) driven by SLO2.1. To assess the presence of K_{Na} currents in MSMCs isolated from non-pregnant mice, we first conducted single-channel recordings, revealing Na^+-activated K^+ channels with an approximate conductance of 100 pS, likely the Na^+-activated K^+ channel SLO2.1 (Figure 2a and 2b). We also detected activity (not shown) of the large-conductance Ca^{2+}-activated K^+ channel SLO1 (BK_{Ca}, encoded by *Kcnma1*), which is expressed in MSMCs (Brainard et al., 2009; Ferreira et al., 2019; Khan et al., 1993, 1998; Lorca et al., 2014; Wakle-Prabagaran et al., 2016). We next performed whole-cell patch clamp experiments in which we applied depolarizing voltage clamp steps (10 mV) from -80 mV to +120 mV (Vh= 0 mV) in MSMCs. This revealed a time-dependent, non-inactivating outward K^+ current (Figure 2c). We suspected that a portion of this current was conducted by SLO1 (Brainard et al., 2009; Ferreira et al., 2019; Khan et al., 1993, 1998; Lorca et al., 2014; Wakle-Prabagaran et al., 2016), so we treated MSMCs from non-pregnant and d18.5 mice with the SLO1 blocker tetraethylammonium (TEA) (5 mM) (Figure 2c, d). These experiments revealed a TEA-sensitive current (60–70% of the total whole-cell current) and a TEA-resistant current (30-40% of the total whole-cell K^+ current). To confirm that the TEA-resistant current was conducted by SLO2.1, we treated cells with phorbol 12-myristate 13-acetate (PMA). PMA activates protein kinase C, which inhibits SLO21, so PMA is an indirect inhibitor of SLO2.1 (Chen et al., 2009; Kaczmarek, 2013; Santi et al., 2006). PMA inhibited the TEA-resistant current in MSMCs from both

non-pregnant and d18.5 mice (Figure 2c). We conclude that SLO2.1 channels are responsible for the TEA-resistant K^+ current in mouse MSMCs. Consistent with our expression data, SLO2.1 current was lower in MSMCs from d18.5 mice than in MSMCs from non-pregnant mice.

3.3. SLO2.1 and NALCN co-localize in mouse MSMCs. SLO2.1 and other Na^+ channels form complexes in neurons (Hage & Salkoff, 2012; Takahashi & Yoshino, 2015) and SLO2.1 and NALCN form a complex in human MSMCs (Ferreira et al., 2021). To determine whether NALCN co-localizes with SLO2.1 in mouse MSMCs, we conducted *in situ* proximity ligation assays in which we stained mouse MSMCs with antibodies recognizing SLO2.1 and NALCN, along with DNA-tagged secondary antibodies. If the proteins were within 40 nm, DNA ligation and subsequent amplification would occur, leading to fluorescent punctae in the cells. We observed significantly more punctae in cells stained with both anti-NALCN and anti-SLO2.1 antibodies than in cells stained with either antibody alone or with only secondary antibodies (Figure 3). This finding indicates that NALCN and SLO2.1 co-localize in mouse MSMCs.

3.4. Na^+ influx through NALCN activates SLO2.1 in MSMCs from non-pregnant and early pregnant mice. To determine whether Na^+ influx through NALCN activates SLO2.1 in mouse MSMCs as in human MSMCs (Ferreira et al., 2021), we conducted whole-cell patch clamp experiments on MSMCs isolated from different stages of pregnancy. Substituting 135 mM Li^+ with 135 mM extracellular Na^+ led to a 100–200% increase in K^+ currents at both +80 mV and -60 mV in MSMCs from non-pregnant and early pregnant (d7.5) mice but not in MSMCs from d14.5 and d18.5 (Figure 4a, c, d). To determine whether the channel responsible for conducting Na^+ to activate SLO2.1 was NALCN, we conducted similar experiments in non-pregnant mouse MSMCs expressing shRNA specific to NALCN (Figure 4b and Supplementary figure 2). In these cells, the K_{Na} current activated by Na^+ was 10-20% of that in control MSMCs (Figure 4b, c, d). Additionally, Gd^{2+} and NALCN inhibitors significantly inhibited this current (Supplementary figure 2). These findings suggest that, in non-pregnant and early pregnancy stages, the Na^+ responsible for activating K^+ efflux through SLO2.1 enters MSMCs through NALCN.

3.5. Activation of the NALCN/SLO2.1 complex hyperpolarizes MSMCs from non-pregnant and early pregnancy stage mice. We next wondered whether Na^+-mediated activation of SLO2.1 and the ensuing K^+ efflux could lead to membrane hyperpolarization in mouse MSMCs. Thus, we performed flow cytometry with the cationic voltage-sensitive dye, DiSC3(5) (Ferreira et al., 2021). In MSMCs from non-pregnant and d7.5 mice, treatment with 80 mM extracellular Na^+ led to a respective increase of 28.22 +/- 26.15 and 30.14 +/- 13.49 in DiSC3(5) fluorescence (normalized to Valinomycin), indicating membrane hyperpolarization at these stages (Figure 5b, d). Treatment with 80 mM Li^+, a NALCN-permeable cation that does not activate SLO2.1, depolarized MSMCs from non-pregnant mice (Figure 5c). Similar experiments with the impermeable cation Choline also showed no membrane hyperpolarization, indicating that the Na^+ effect was not due to osmolarity changes (Ferreira et al. 2021). Conversely, MSMCs from d14.5 and d18.5 mice exhibited a statistically significant depolarization after addition of 80 mM Na^+ (Figure 5b, d). This indicated that Na^+ influx at these stages did not activate K^+ efflux through SLO2.1.

To confirm that SLO2.1 and NALCN contribute to the Na^+-induced membrane hyperpolarization, we isolated MSMCs from mice expressing shRNAs specific for *Slo2.1*

or *Nalcn*. These MSMCs exhibited significantly smaller Na^+-dependent membrane hyperpolarization than those that received scrambled shRNA control (Figure 5e). Consistent with these findings, treatment with PMA resulted in Na^+-dependent depolarization, and treatment with Gd^{2+} or NALCN inhibitors prevented activation of SLO2.1 by Na^+ influx (Supplemental figure 3). Together, our results suggest that Na^+ influx through NALCN activates SLO2.1-dependent membrane hyperpolarization in mouse MSMCs.

3.6 SLO2.1 and NALCN differentially modulate Ca^{2+} responses in mouse MSMCs across pregnancy. Membrane depolarization in human and mouse MSMCs enhances Ca^{2+} influx via VDCCs (Ferreira et al., 2021),and inhibiting SLO2.1 in human MSMCs leads to increased Ca^{2+} entry through VDCCs (Ferreira et al., 2019, 2021). Thus, we wanted to define the effects of the NALCN/SLO2.1 complex on Ca^{2+} in mouse MSMCs across pregnancy. To do so, we loaded MSMCs with the Ca^{2+} indicator Fluo4-AM. Treatment of MSMCs from non-pregnant mice with 135 mM Li^+ induced similar Ca^{2+} oscillations (Figure 6b, c) as those prompted by 50 mM KCl (Figure 6a), whereas 135 mM Na^+ abolished these oscillations (not shown). Treatment of MSMCs from non-pregnant mice in which *Slo2.1* or *Nalcn* were knocked down caused no Ca^{2+} oscillations, indicating that the oscillations depended on the two channels (Figure 6d). Similarly, Li^+-induced Ca^{2+} oscillations were significantly reduced in cells treated with NALCN inhibitors (Supplementary figure 4). Conversely, treatment with 135 mM Li^+ did not induce Ca^{2+} oscillations in MSMCs from pregnancy d18.5 mice (Figure 6c, d, and e).

To confirm that the Ca^{2+} oscillations depended on extracellular Ca^{2+}, we repeated the experiment in 0 mM extracellular Ca^{2+} plus 2 mM EGTA. This treatment prevented the Li^+-induced Ca^{2+} oscillations (Supplementary Figure 4). Furthermore, the proportion of cells responding to Li^+ was lower when the VDCC inhibitor Verapamil was present (Figure 6e). In summary, our results indicate that Na^+ influx through NALCN activates SLO2.1, leading to membrane hyperpolarization and reduction of Ca^{2+} oscillations in MSMCs from non-pregnant and early pregnancy stage mice but not in MSMCs from late-pregnancy stage mice.

4. Discussion

Previous work showed that the Na^+ channel NALCN and the K^+ channel SLO2.1 form a functional complex that regulates human MSMC membrane potential at the end of pregnancy. Here, we present several lines of evidence indicating that NALCN and SLO2.1 form a functional complex that modulates mouse MSMC membrane potential and excitability throughout all stages of pregnancy. First, we show that SLO2.1 and NALCN mRNA and protein were expressed in mMSMCs throughout pregnancy. Their expression declined in late pregnancy, aligning with the higher MSMC excitability observed at this stage. Second, we show that SLO2.1 currents constitute a significant portion of the total K^+ current in mouse MSMCs. SLO2.1 currents are reduced in late pregnancy, corroborating our expression data. Third, we demonstrate that NALCN and SLO2.1 are in spatial proximity within mouse MSMC membranes. Fourth, knocking down NALCN resulted in a nearly complete reduction of the of the Na^+-activated SLO2.1 currents in mouse MSMCs. Fifth, in non-pregnant and early pregnancy stages, SLO2.1 activation led to membrane hyperpolarization, primarily driven by Na^+ influx through NALCN. In late pregnancy and in SLO2.1 or NALCN knockdown non-pregnant animals, Na^+ influx

promoted membrane depolarization instead of hyperpolarization. Finally, we report that SLO2.1/NALCN activity regulated Ca^{2+} entry through VDCCs in MSMCs from non-pregnant or early pregnancy mice, and that this Ca^{2+} entry is significantly reduced in MSMCs from mice in late pregnancy. Together, our findings indicate that activation of SLO2.1 by Na^{+} carried by NALCN is important for regulating uterine quiescence by modulating the resting membrane potential during early pregnancy and in non-pregnant animals.

Our data are in agreement with previous studies in human, rat, and mouse myometrial smooth muscle cells (MSMCs) demonstrating a transition from a hyperpolarized state to a depolarized state (Casteels & Kuriyama, 1965; OSA, 1974; Parkington et al., 1999). This depolarization activates L-type voltage–dependent calcium (Ca^{2+}) channels, which allow an influx of Ca^{2+} to both generate an action potential and activate actomyosin contractile machinery (Berridge, 2008). Our mouse model provides insights into NALCN's potential role in regulating myometrial activity across pregnancy stages. Contrary to previous findings (Reinl et al., 2015b), which suggested a direct effect of NALCN on the muscle inter-burst frequency, our study suggests that NALCN primary role is to modulate K^{+} permeability, especially through its interaction with SLO2.1 (Ferreira et al., 2021). In addition to NALCN, other Na^{+} channels such as the TRPC 1, 3 and 6 (Babich et al., 2004; Dalrymple, 2002; Dalrymple et al., 2007; Ku et al., 2006; Lacampagne et al., 1994; Wang et al., 2020; Yang & Sachs, 1989) are expressed in MSMC. However, these channels appear to have a minimal contribution to Na^{+}-activated hyperpolarization in human MSMCs (Ferreira et al., 2021).

In addition to SLO2, other K^{+} channels such as Kir7.1 and SLO1 are also expressed in mouse MSMCs (Brainard et al., 2007; Ferreira et al., 2019; Khan et al., 1993; McCloskey et al., 2014). SLO1 channels exhibit high-voltage sensitivity, decreasing their contribution to currents at the resting membrane potential. Kir7.1 channels maintain a hyperpolarized resting membrane potential and low excitability in both mouse and human uterine tissue, peaking in mid-pregnancy in mice (McCloskey et al., 2014). Thus, Kir7.1 could play a role in regulating the hyperpolarized resting membrane potential to maintain uterine quiescence in early pregnancy. However, our study demonstrates that SLO1 and SLO2.1 together contribute to approximately 90% of the K^{+} current in mouse MSMCs, similar to observations in human MSMCs (Ferreira et al., 2019). Further research is needed to fully elucidate the roles of Kir7.1 and TRP channels in mouse MSMCs.

Interestingly, our data also revealed that both *Nalcn and SLO2.1* expression are highest d7.5 in the pregnancy. At this stage of pregnancy, the myometrium is undergoing proliferation, a process that is controlled by ion channel activity. Two recent studies have suggested NALCN may contribute to proliferation. The first found that overexpression of NALCN increases Ca^{2+} oscillations in prostate cancer promoting invasion and metastasis (Folcher et al., 2023) In contrast, Rahrmann et. al, found that loss of NALCN increased the growth of gastric cancer spheroids *in vitro* and cell shedding and metastasis *in vivo* (Rahrmann et al., 2022). More investigation is needed to understand if NALCN alone, or in combination with SLO2.1 is critical for MSMC proliferation at this early stage of pregnancy. Furthermore, several NALCN accessory subunits have been identified and are thought to be necessary for NALCN function and localization on the plasma

membrane, including Nalf1. The role of accessory subunits will be the subject of future investigation.

In summary, we demonstrate that the SLO2.1/NALCN functional complex is conserved between mice and humans and functions throughout pregnancy. Future studies should investigate the hormonal modulation of these channels in mice. In human MSMCs, progesterone regulates the expression of NALCN (Amazu et al., 2020), and oxytocin inhibits SLO2.1 activity (Ferreira et al., 2021). Additional studies should also focus on the interactions with other ion channels and the regulation of NALCN by accessory proteins. Such research could lead to novel drug targets for modulating myometrial contractility.

Figures.

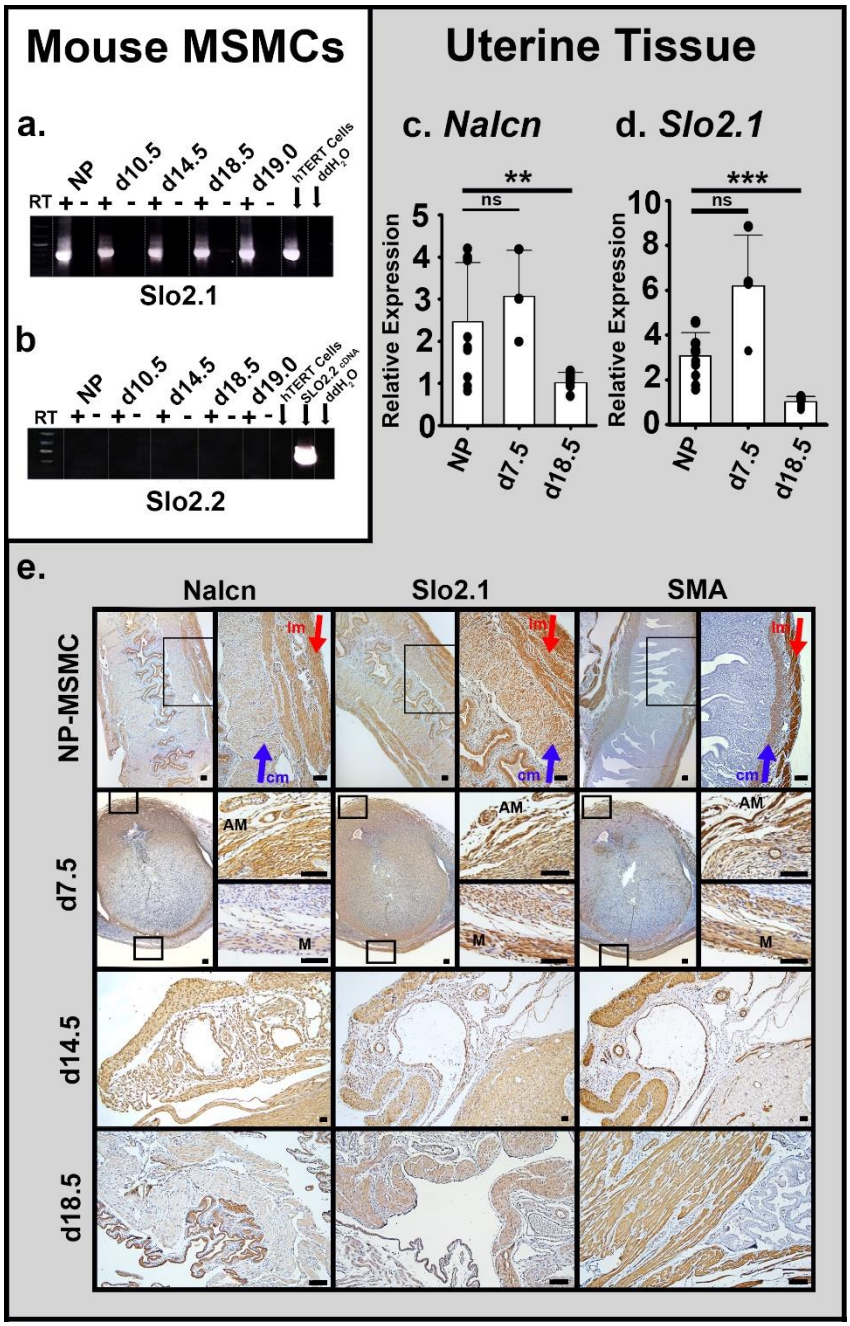

Figure 1. SLO2.1 and NALCN expression in uterus and myometrial smooth muscle cells. (**a** and **b**) Representative reverse transcription PCR of Slo2.1 (**a**) or Slo2.2 (**b**) in myometrial smooth muscle cells (MSMCs) from non-pregnant (NP) and day post coitus (d), 10.5, 14.5, 18.5, and 19 mice. No reverse transcriptase (RT) and ddH_2O are negative controls, hTERT cell cDNA is a positive control. (**c** and **d**) Relative mRNA expression of Nalcn (**c**) and Slo2.1 (**d**) in mouse uteri as measured by quantitative real-time PCR. Expression was normalized to *Top1* and *Sdha*. (**e**) Immunohistochemistry of NALCN and SLO2.1 in mouse uteri at the indicated time points, with hematoxylin counterstain. SMA, smooth muscle actin. Scale bar, 100μm. lm, longitudinal muscle; cm, circular muscle; AM, antimesometrial; M, mesometrial.

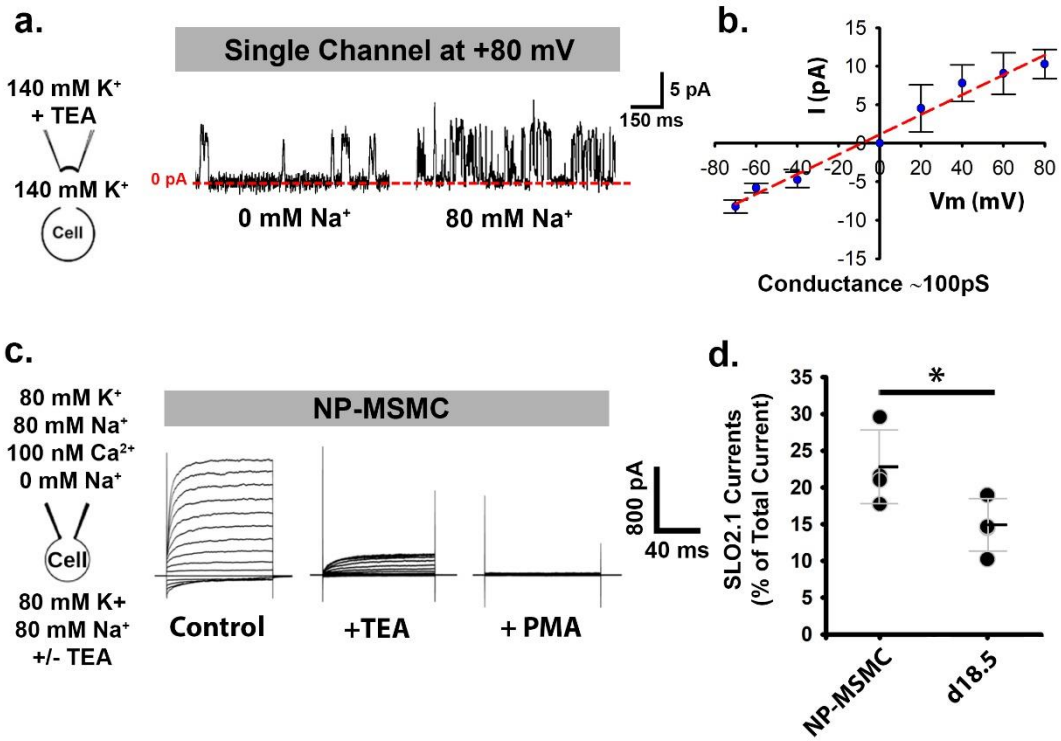

Figure 2. SLO2.1 Sodium-activated potassium currents in mMSMCs. (**a**) Single channel patch-clamp schematic and recordings of SLO2.1 channels from MSMCs from non-pregnant mice. (**b**) Graph showing the amplitude of the Na^+-sensitive K^+ channels in mouse MSMCs. (**c**) Whole-cell patch clamp schematic and K^+ currents recorded from MSMCs at +80 mV (Vh =0 mV, with step pulses from −80 to +120 mV) with no additives (control), in the presence of 5 mM TEA in the external solution (+TEA), and in the prescence of 1 μM PMA (+PMA). **(d)** Graph showing the percentages of SLO2.1 currents (PMA-sensitive currents) from MSMCs from nonpregnant (NP) mice and pregnancy day 18.5 females (22.48 ± 5.02, n=4 and 14.58 ± 3.57, n=4, respectively). *P <0.05 by unpaired t-test.

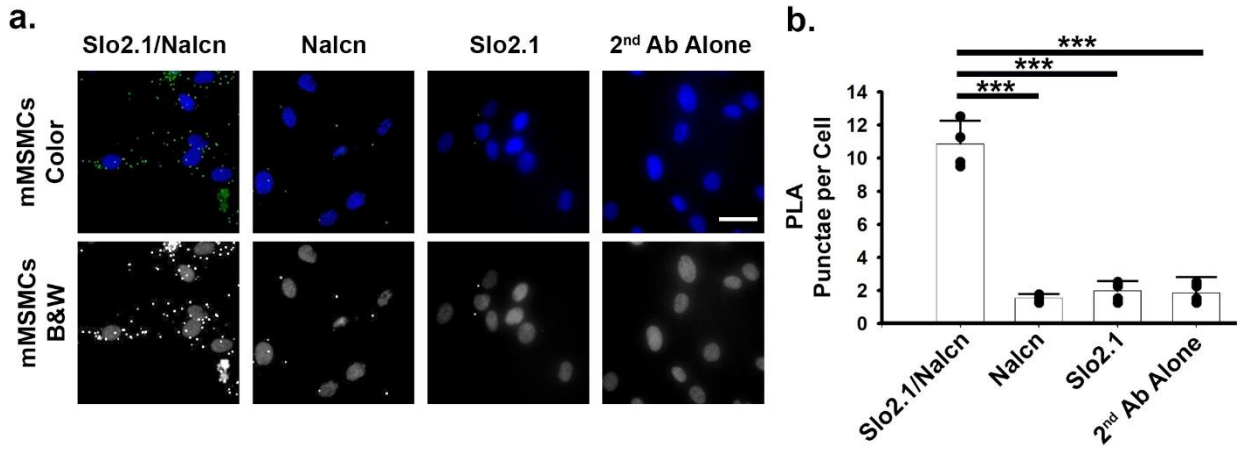

Figure 3. SLO2.1 and NALCN colocalization in mouse MSMCs. (**a**) Representative proximity ligation assay labeling (green) of mouse MSMCs with the indicated single antibodies and antibody combinations. Blue is nuclear stain. Scale bar, 20 μm. (**b**) Average number of punctae in mouse MSMCs with the indicated antibodies. The values are: SLO2.1/NALCN, 10.75 ± 1.40, n = 4; NALCN, 1.44 ± 0.24, n = 4; SLO2.1, 1.87 ± 0.59, n = 4; and 2nd Ab Alone, 1.75 ± 0.95, n = 4. Over 100 cells per condition were counted. Data are presented as mean and standard deviation. ***$P < 0.001$ by unpaired t test.

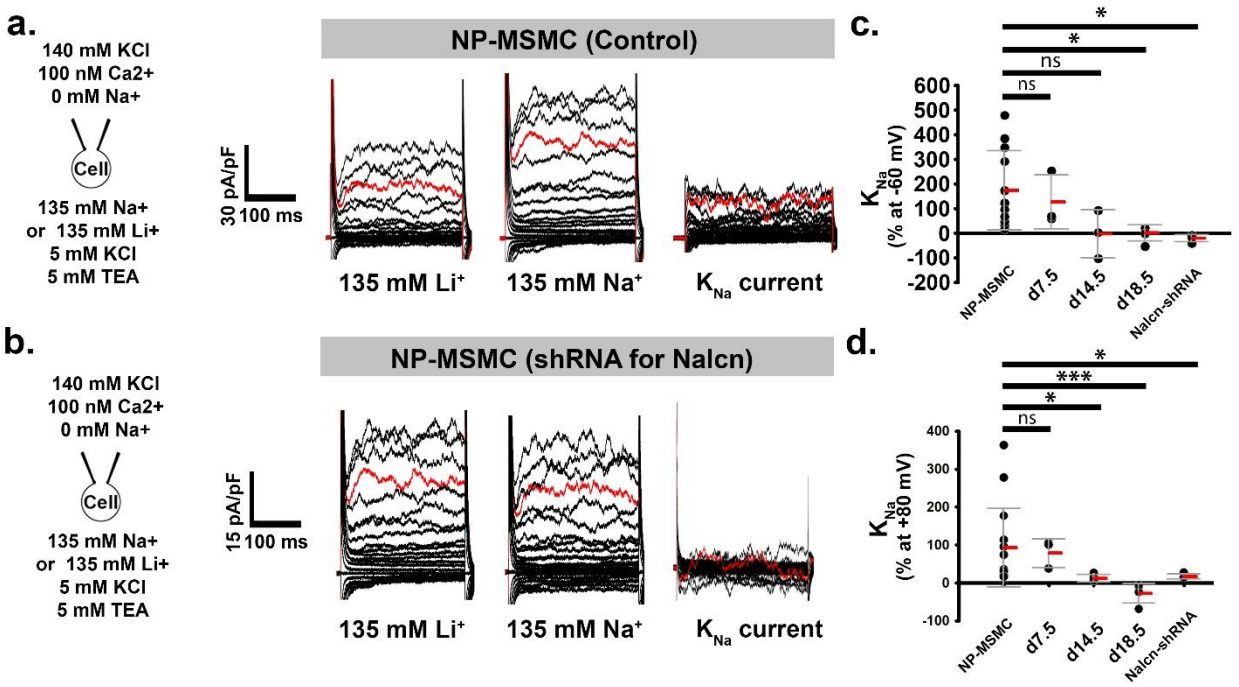

Figure 4. SLO2.1 channel activation by an NALCN-dependent Na^+ current in mouse MSMCs. (**a** and **b**) Left, schematics of whole-cell bath and pipette ionic concentrations. Right, representative whole-cell currents elicited from Vh = -70 mV, and step pulses from -80 to +120 mV, recorded in 135 mM Na^+ or 135 mM external Li^+ of MSMCs isolated from non-pregnant (NP) mice or NP mice treated with NALCN-shRNA. The Na^+-dependent currents were calculated by subtracting traces (135 mM Na^+ – 135 mM Li^+). (**c** and **d**) Graphs depicting the percentage of Na^+-dependent currents at -60 mV and +80 mV, respectively. Data are plotted as the mean and standard deviation. (**c**) Values are: NP, 173.63 ± 161.17, n= 15; d7.5, 126.58 ± 109.35, n= 3; d14.5, -3.04 ± 97.59, n= 3; d18.5, 0.62 ± 31.85, n= 5; and NALCN shRNA, -20.77 ± 14.23, n= 4. (**d**) Values are; NP, 93.50 ± 105.39, n= 15; d7.5, 81.28 ± 37.65, n= 3; d14.5, 14.83 ± 10.39, n= 3; d18.5, -25.01 ± 25.43, n= 5; and NALCN shRNA, 18.54 ± 21.41, n= 4. *$P < 0.05$, **$P < 0.01$, ***$P < 0.001$ by unpaired t-test with or without Mann-Whitney corrections.

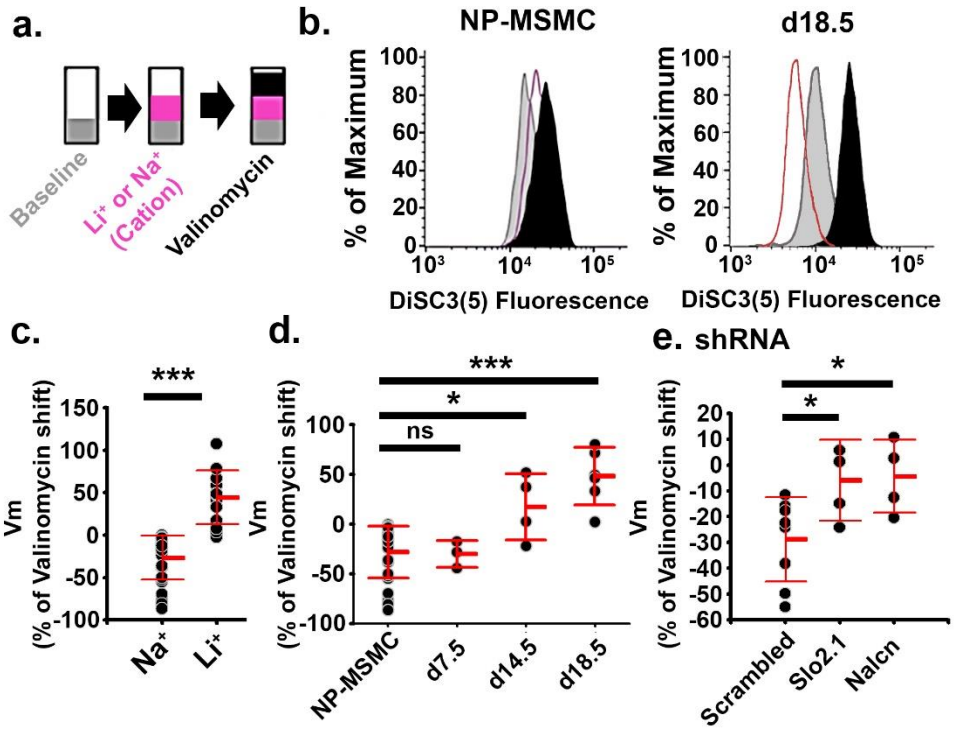

Figure 5. Myometrial smooth muscle cell membrane potential regulation by SLO2.1 and NALCN. (**a**) Experimental scheme. (**b**) Representative images of relative shifts of DiSC3(5) fluorescence induced by 80 mM Na^+ in MSMCs from non-pregnant (NP) and pregnancy day (d) 18.5 mice. (**c**) Quantification of shifts induced by Na^+ (-28.22 ± 26.16, n= 27), and Li^+ (42.83 ± 31.54, n= 13) in MSMCs from NP mice. (**d**) Quantification of shifts induced by Na^+. Values are NP, -28.22 ± 26.16, n= 27; d7.5, -30.14 ± 13.49, n=3; d14.5, 17.23 ± 33.27, n=4; and d18.5, 48.18 ± 29.09, n=10. (**e**) Quantification of shifts induced by Na^+ in NP mice treated with shRNA for SLO2.1 (-6.40 ± 15.70, n=4), NALCN (-4.91 ± 14.15, n=4), and Scrambled (-29.35 ± 16.31, n=8). (**c to e**) All data were normalized to the fluorescence changes induced by valinomycin and are presented as mean and standard deviation. $^{**}P < 0.01$, $^{***}P < 0.001$ by unpaired t-test with Mann-Whitney corrections.

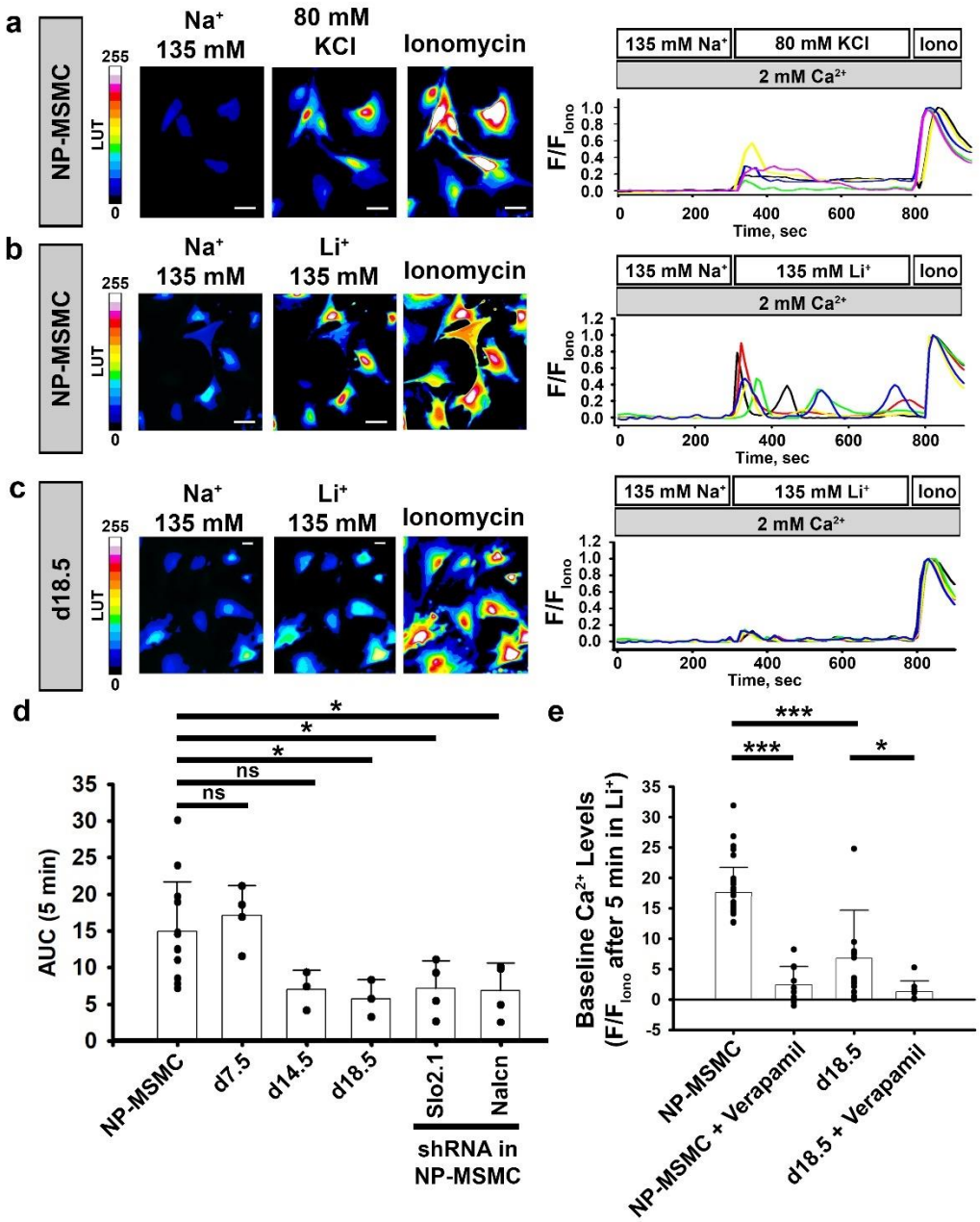

Figure 6. SLO2.1/NALCN regulation of intracellular calcium homeostasis in mouse MSMCs. (**a to c**) Representative fluorescence images (left) and quantitation (right) from MSMCs from non-pregnant (NP) and pregnancy day (d) 18.5 mice loaded with 10 μM Fluo-4 AM in the presence of the indicated ions. (**d**) Graph of the areas under the curve (AUC) of the first 5 min after changing the solutions from 135 mM Na^+ to 135 mM Li^+. Values are: NP, 14.78 ± 6.74, n= 13; d7.5, 17.02 ± 4.05, n= 4; d14.5, 6.93 ± 2.63, n= 4; d18.5, 5.73 ± 2.55, n= 3; SLO2.1 shRNA, 7.09 ± 3.78, n= 4; and NALCN shRNA, 6.82 ± 3.74, n= 4. (**e**) Graph of the baseline Ca^{2+} in NP and d18.5 mice, in control conditions and in the presence of the voltage-activated calcium channel inhibitor verapamil. Values are: NP, 17.65 ± 4.15, n=13; NP + Verapamil, 2.42 ± 3.02, n= 4; d18.5, 6.81 ± 7.93, n=

4; and d18.5 + Verapamil, 1.33 ± 1.76, n= 4. All data were normalized to the fluorescence in 2-5 μM ionomycin and 2 mM extracellular Ca^{2+} (Iono), and all data are presented as mean and standard deviation. *P < 0.05, and *** P < 0.001 by unpaired t-test with or without Mann-Whitney corrections.

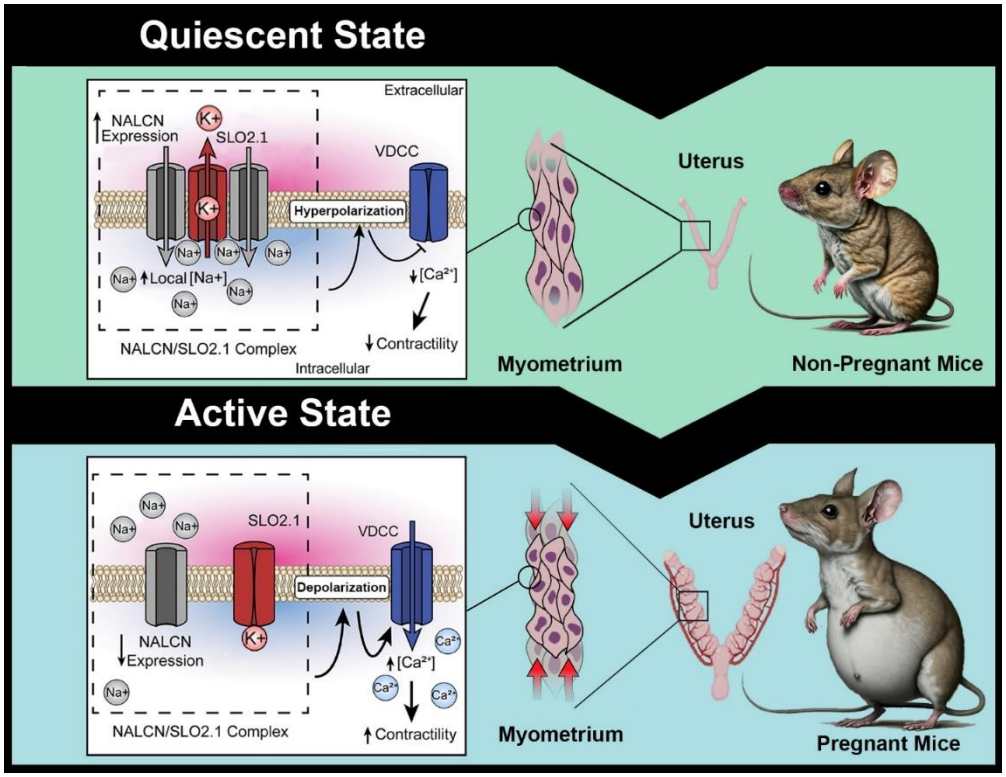

Figure 7. Proposed model by which the SLO2.1/NALCN complex regulates myometrial excitability during pregnancy in mice. In non-pregnant mice and during early pregnancy ("quiescent state") Na^+ current through NALCN activates SLO2.1 channels, increasing K^+ efflux to maintain the cell in a hyperpolarized state. As a result, voltage dependent Ca^{2+} channels (VDCCs) are closed, and the uterus is quiescent. At the end of pregnancy ("active state"), expression of NALCN and SLO2.1 channels and SLO2.1 activity are reduced. The reduced K^+ efflux depolarizes the membrane, leading to VDCC activation, an increase in intracellular Ca^{2+}, and uterine contractility. Image modified from Ferreira et al 2021, https://doi.org/10.1016/ j.isci.2021.103210.

References.

Amazu, C., Ma, X., Henkes, C., Ferreira, J. J., Santi, C. M., & England, S. K. (2020). Progesterone and estrogen regulate NALCN expression in human myometrial smooth muscle cells. *American Journal of Physiology-Endocrinology and Metabolism*, *318*(4), E441–E452. https://doi.org/10.1152/ajpendo.00320.2019

Anwer, K., Oberti, C., Perez, G. J., Perez-Reyes, N., McDougall, J. K., Monga, M., Sanborn, B. M., Stefani, E., & Toro, L. (1993). Calcium-activated K+ channels as modulators of human myometrial contractile activity. *American Journal of Physiology-Cell Physiology*, *265*(4), C976–C985. https://doi.org/10.1152/ajpcell.1993.265.4.C976

Babich, L. G., Ku, C.-Y., Young, H. W. J., Huang, H., Blackburn, M. R., & Sanborn, B. M. (2004). Expression of Capacitative Calcium TrpC Proteins in Rat Myometrium During Pregnancy1. *Biology of Reproduction*, *70*(4), 919–924. https://doi.org/10.1095/biolreprod.103.023325

Berridge, M. J. (2008). Smooth muscle cell calcium activation mechanisms. *The Journal of Physiology*, *586*(21), 5047–5061. https://doi.org/10.1113/jphysiol.2008.160440

Brainard, A. M., Korovkina, V. P., & England, S. K. (2007). Potassium channels and uterine function. *Seminars in Cell & Developmental Biology*, *18*(3), 332–339. https://doi.org/10.1016/j.semcdb.2007.05.008

Brainard, A. M., Korovkina, V. P., & England, S. K. (2009). Disruption of the maxi-K-caveolin-1 interaction alters current expression in human myometrial cells. *Reproductive Biology and Endocrinology*, *7*(1), 131. https://doi.org/10.1186/1477-7827-7-131

Casteels, R., & Kuriyama, H. (1965). Membrane potential and ionic content in pregnant and non-pregnant rat myometrium. *The Journal of Physiology*, *177*(2), 263–287. https://doi.org/10.1113/jphysiol.1965.sp007591

Chen, H., Kronengold, J., Yan, Y., Gazula, V.-R., Brown, M. R., Ma, L., Ferreira, G., Yang, Y., Bhattacharjee, A., Sigworth, F. J., Salkoff, L., & Kaczmarek, L. K. (2009). The N-Terminal Domain of Slack Determines the Formation and Trafficking of Slick/Slack Heteromeric Sodium-Activated Potassium Channels. *The Journal of Neuroscience*, *29*(17), 5654–5665. https://doi.org/10.1523/JNEUROSCI.5978-08.2009

Dalrymple, A. (2002). Molecular identification and localization of Trp homologues, putative calcium channels, in pregnant human uterus. *Molecular Human Reproduction*, *8*(10), 946–951. https://doi.org/10.1093/molehr/8.10.946

Dalrymple, A., Mahn, K., Poston, L., Songu-Mize, E., & Tribe, R. M. (2007). Mechanical stretch regulates TRPC expression and calcium entry in human myometrial smooth muscle cells. *MHR: Basic Science of Reproductive Medicine*, *13*(3), 171-179*. https://doi.org/10.1093/molehr/gal110

Ferreira, J. J., Amazu, C., Puga-Molina, L. C., Ma, X., England, S. K., & Santi, C. M. (2021). SLO2.1/NALCN a sodium signaling complex that regulates uterine activity. *IScience*, *24*(11), 103210. https://doi.org/10.1016/j.isci.2021.103210

Ferreira, J. J., Butler, A., Stewart, R., Gonzalez-Cota, A. L., Lybaert, P., Amazu, C., Reinl, E. L., Wakle-Prabagaran, M., Salkoff, L., England, S. K., & Santi, C. M. (2019). Oxytocin can regulate myometrial smooth muscle excitability by inhibiting the Na^+-activated K^+

channel, Slo2.1. *The Journal of Physiology*, *597*(1), 137–149. https://doi.org/10.1113/JP276806

Folcher, A., Gordienko, D., Iamshanova, O., Bokhobza, A., Shapovalov, G., Kannancheri-Puthooru, D., Mariot, P., Allart, L., Desruelles, E., Spriet, C., Diez, R., Oullier, T., Marionneau-Lambot, S., Brisson, L., Geraci, S., Impheng, H., Lehen'kyi, V., Haustrate, A., Mihalache, A., … Prevarskaya, N. (2023). <scp>NALCN</scp> -mediated sodium influx confers metastatic prostate cancer cell invasiveness. *The EMBO Journal*, *42*(13). https://doi.org/10.15252/embj.2022112198

Hage, T. A., & Salkoff, L. (2012). Sodium-Activated Potassium Channels Are Functionally Coupled to Persistent Sodium Currents. *The Journal of Neuroscience*, *32*(8), 2714–2721. https://doi.org/10.1523/JNEUROSCI.5088-11.2012

Kaczmarek, L. K. (2013). Slack, Slick, and Sodium-Activated Potassium Channels. *ISRN Neuroscience*, *2013*, 1–14. https://doi.org/10.1155/2013/354262

Khan, R. N., Morrison, J. J., Smith, S. K., & Ashford, M. L. J. (1998). Activation of large-conductance potassium channels in pregnant human myometrium by pinacidil. *American Journal of Obstetrics and Gynecology*, *178*(5), 1027–1034. https://doi.org/10.1016/S0002-9378(98)70543-5

Khan, R. N., S K Smith, J J Morrison, & M L Ashford. (1993). Properties of large-conductance K+ channels in human myometrium during pregnancy and labour. *Proceedings of the Royal Society of London. Series B: Biological Sciences*, *251*(1330), 9–15. https://doi.org/10.1098/rspb.1993.0002

Knock, G. A., Smirnov, S. V., & Aaronson, P. I. (1999). Voltage-gated K^+ currents in freshly isolated myocytes of the pregnant human myometrium. *The Journal of Physiology*, *518*(3), 769–781. https://doi.org/10.1111/j.1469-7793.1999.0769p.x

Ku, C. Y., Babich, L., Word, R. A., Zhong, M., Ulloa, A., Monga, M., & Sanborn, B. M. (2006). Expression of Transient Receptor Channel Proteins in Human Fundal Myometrium in Pregnancy. *Journal of the Society for Gynecologic Investigation*, *13*(3), 217–225. https://doi.org/10.1016/j.jsgi.2005.12.007

Lacampagne, A., Gannier, F., Argibay, J., Garnier, D., & Le Guennec, J.-Y. (1994). The stretch-activated ion channel blocker gadolinium also blocks L-type calcium channels in isolated ventricular myocytes of the guinea-pig. *Biochimica et Biophysica Acta (BBA) - Biomembranes*, *1191*(1), 205–208. https://doi.org/10.1016/0005-2736(94)90250-X

Lorca, R. A., Prabagaran, M., & England, S. K. (2014). Functional insights into modulation of BKCa channel activity to alter myometrial contractility. *Frontiers in Physiology*, *5*. https://doi.org/10.3389/fphys.2014.00289

McCloskey, C., Rada, C., Bailey, E., McCavera, S., van den Berg, H. A., Atia, J., Rand, D. A., Shmygol, A., Chan, Y., Quenby, S., Brosens, J. J., Vatish, M., Zhang, J., Denton, J. S., Taggart, M. J., Kettleborough, C., Tickle, D., Jerman, J., Wright, P., … Blanks, A. M. (2014). The inwardly rectifying K^+ channel <scp>KIR</scp> 7.1 controls uterine excitability throughout pregnancy. *EMBO Molecular Medicine*, *6*(9), 1161–1174. https://doi.org/10.15252/emmm.201403944

OSA, T. (1974). AN INTERACTION BETWEEN THE ELECTRICAL ACTIVITIES OF LONGITUDINAL AND CIRCULAR SMOOTH MUSCLES OF PREGNANT MOUSE UTERUS. *The Japanese Journal of Physiology*, *24*(2), 189–203. https://doi.org/10.2170/jjphysiol.24.189

Parkington, H. C., Tonta, M. A., Brennecke, S. P., & Coleman, H. A. (1999). Contractile activity, membrane potential, and cytoplasmic calcium in human uterine smooth muscle in the third trimester of pregnancy and during labor. *American Journal of Obstetrics and Gynecology*, *181*(6), 1445–1451. https://doi.org/10.1016/S0002-9378(99)70390-X

Rahrmann, E. P., Shorthouse, D., Jassim, A., Hu, L. P., Ortiz, M., Mahler-Araujo, B., Vogel, P., Paez-Ribes, M., Fatemi, A., Hannon, G. J., Iyer, R., Blundon, J. A., Lourenço, F. C., Kay, J., Nazarian, R. M., Hall, B. A., Zakharenko, S. S., Winton, D. J., Zhu, L., & Gilbertson, R. J. (2022). The NALCN channel regulates metastasis and nonmalignant cell dissemination. *Nature Genetics*, *54*(12), 1827–1838. https://doi.org/10.1038/s41588-022-01182-0

Reinl, E. L., Cabeza, R., Gregory, I. A., Cahill, A. G., & England, S. K. (2015a). Sodium leak channel, non-selective contributes to the leak current in human myometrial smooth muscle cells from pregnant women. *Molecular Human Reproduction*, *21*(10), 816–824. https://doi.org/10.1093/molehr/gav038

Reinl, E. L., Cabeza, R., Gregory, I. A., Cahill, A. G., & England, S. K. (2015b). Sodium leak channel, non-selective contributes to the leak current in human myometrial smooth muscle cells from pregnant women. *Molecular Human Reproduction*, *21*(10), 816–824. https://doi.org/10.1093/molehr/gav038

Reinl, E. L., Zhao, P., Wu, W., Ma, X., Amazu, C., Bok, R., Hurt, K. J., Wang, Y., & England, S. K. (2018). Na+-Leak Channel, Non-Selective (NALCN) Regulates Myometrial Excitability and Facilitates Successful Parturition. *Cellular Physiology and Biochemistry*, *48*(2), 503–515. https://doi.org/10.1159/000491805

Santi, C. M., Ferreira, G., Yang, B., Gazula, V.-R., Butler, A., Wei, A., Kaczmarek, L. K., & Salkoff, L. (2006). Opposite Regulation of Slick and Slack K^+ Channels by Neuromodulators. *The Journal of Neuroscience*, *26*(19), 5059–5068. https://doi.org/10.1523/JNEUROSCI.3372-05.2006

Takahashi, I., & Yoshino, M. (2015). Functional coupling between sodium-activated potassium channels and voltage-dependent persistent sodium currents in cricket Kenyon cells. *Journal of Neurophysiology*, *114*(4), 2450–2459. https://doi.org/10.1152/jn.00087.2015

Wakle-Prabagaran, M., Lorca, R. A., Ma, X., Stamnes, S. J., Amazu, C., Hsiao, J. J., Karch, C. M., Hyrc, K. L., Wright, M. E., & England, S. K. (2016). BK $_{Ca}$ channel regulates calcium oscillations induced by alpha-2-macroglobulin in human myometrial smooth muscle cells. *Proceedings of the National Academy of Sciences*, *113*(16). https://doi.org/10.1073/pnas.1516863113

Wang, H., Cheng, X., Tian, J., Xiao, Y., Tian, T., Xu, F., Hong, X., & Zhu, M. X. (2020). TRPC channels: Structure, function, regulation and recent advances in small molecular probes. *Pharmacology & Therapeutics*, *209*, 107497. https://doi.org/10.1016/j.pharmthera.2020.107497

Yang, X.-C., & Sachs, F. (1989). Block of Stretch-Activated Ion Channels in *Xenopus* Oocytes by Gadolinium and Calcium Ions. *Science*, *243*(4894), 1068–1071. https://doi.org/10.1126/science.2466333